Cite as: A. Karton, *Chemical Physics,* 552 (2022) 111373
https://doi.org/10.1016/j.chemphys.2021.111373

Shapeshifting radicals

Amir Karton

School of Molecular Sciences, The University of Western Australia, Perth, WA 6009, Australia.

ABSTRACT

Since the synthesis of bullvalene, closed-shell shapeshifting hydrocarbon cages have been extensively studied both experimentally and theoretically. However, considerably less attention has been given to shapeshifting radical hydrocarbon cages. Despite being synthesized over 30 years ago, the shapeshifting barbaralyl radical $(CH)_9$• has not been studied computationally, and very few experimental studies have been reported. Here, we brush the dust off this shapeshifting radical using the high-level W1-F12 composite ab initio method. We find that consistent with the experimental results, rearrangement of the barbaralyl radical proceeds through a series of β-scission and cyclization steps, which are kinetically favorable over degenerate Cope rearrangements. We proceed to examine these chemical processes in a larger shapeshifting radical cage $(CH)_{11}$•, which has not been previously investigated. This shapeshifting radical involves a more complex set of rearranges through β-scissions and cyclizations and is predicted to be less fluxional than the barbaralyl radical.

Corresponding Author. Tel.: +61 8 6488 3139. E-mail: amir.karton@uwa.edu.au (A. Karton).

Introduction

Ever since bullvalene was hypothesized by Doering and Roth[1] and synthesized shortly thereafter by Schröder,[2] highly fluxional or 'shapeshifting' molecules have captured the imagination of organic chemists.[3,4,5,6,7] Bullvalene is a highly fluxional polycyclic hydrocarbon cage in which the carbon skeleton is continuously changing with no 'permanent' carbon–carbon bonds at finite temperatures. Since the discovery of bullvalene, several shapeshifting hydrocarbon cages have been synthesized. The family of shapeshifting hydrocarbon cages includes the following prototypical molecules: semibullvalene $(CH)_8$, barbaralane C_9H_{10}, and bullvalene $(CH)_{10}$, as well as their ketone derivatives barbaralone (C_9H_8O) and bullvalone ($C_{10}H_{10}O$) (see ref. 3 for a recent review). These closed-shell systems undergo rapid degenerate Cope rearrangements which constantly change their hydrocarbon skeleton, and have been extensively studied both experimentally[8,9,10,11,12,13,14,15,16,17,18] and theoretically.[8,13,19,20,21,22,23,24,25,26,27,28,29,30,31,32,33,34,35] Significantly less attention has been given to shapeshifting radical hydrocarbon cages. To the best of our knowledge, the barbaralyl radical $(CH)_9$• has not been studied computationally, and few experimental studies have been reported.[36,37,38]

The development of reliable and computationally affordable wavefunction and density functional theory (DFT) methods over the past two decades places contemporary quantum chemistry in an ideal position for predicting and exploring new chemistry.[39] Today, quantum chemistry plays a key role in the prediction of new molecules and materials with tailored or novel features and properties.[40,41,42,43] Recent examples, in the context of carbon-rich molecules, include tetravinylallene,[44,45] polytriangulane,[46] gaudienes,[47,48] cyclophanes,[49,50] and cyclo[18]carbon.[51,52] In the present work, we use the highly accurate W1-F12 composite ab initio method[53] to explore the Gibbs free potential energy surface of the shapeshifting $(CH)_9$• radical. We then proceed to explore the potential energy surface of the $(CH)_{11}$• radical, which has not been previously investigated, and predict it will exhibit fluxional behaviour as well. In this context it should be

mentioned that shapeshifting radicals entail unique chemical properties. In contrast to resonance stabilized radicals such as the phenyl radical, in which the radical center is instantaneously delocalized over several carbon atoms, in shapeshifting radicals the dynamic delocalization of the radical center around the molecular cage may be controlled to a certain extent via external factors such as temperature variations and interactions with surrounding molecules.[54]

Computational Details

In order to obtain accurate thermochemical and kinetic properties for the $(CH)_9$• radicals, calculations were carried out using the high-level W1-F12 thermochemical procedure.[53] W1-F12 theory combines explicitly correlated F12 techniques [55] with basis-set extrapolations to approximate the all-electron, relativistic CCSD(T) (coupled-cluster with single, double, and quasiperturbative triple excitations) basis-set limit energy. W1-F12 theory can achieve an accuracy in the sub-kcal mol^{-1} range for enthalpies of formation[53,56,57,58,59] and reaction barrier heights[60,61] involving molecules whose wavefunctions are dominated by dynamical correlation. The computational protocol of W1-F12 theory has been specified and rationalized in detail in ref. 53, the following gives a brief overview of the various steps in the W1-F12 thermochemical protocol. The Hartree–Fock (HF) and valence CCSD-F12 correlation energies are extrapolated from the VDZ-F12 and VTZ-F12 basis sets.[62] The complementary auxiliary basis set (CABS) singles correction is included in the HF energy.[63,64,65] The (T) valence correlation energy is extrapolated from the jul-cc-pVDZ and jul-cc-pVTZ basis sets.[66,67,68,69] The CCSD inner-shell contribution is calculated with the core-valence weighted correlation-consistent cc-pwCVTZ basis set,[70] whilst the (T) inner-shell contribution is calculated with the cc-pwCVTZ(no f) basis set (where cc-pwCVTZ(no f) indicates the cc-pwCVTZ basis set without the f functions). The scalar relativistic contribution is obtained at the CCSD(T)/aug-cc-pVDZ-DK level of theory.[71,72,73] All the HF and CCSD(T) calculations employ the restricted open-shell formalism and were

carried out with the Molpro 2016.1 program suite.[74] The geometries for the W1-F12 calculations were optimized at the B3LYP-D3/Def2-TZVPP level of theory as prescribed in the W1-F12 protocol.[53,75,76,77,78,79] Empirical D3 dispersion corrections[80,81] are included using the Becke–Johnson[82] damping potential as recommended in ref. 78. Harmonic vibrational frequency analyses were performed at the same level of theory to confirm that all equilibrium structures have all real frequencies and the transition structures have only one imaginary frequency. The connectivities of the transition structures were confirmed by performing intrinsic reaction coordinate (IRC) calculations.[83,84] Zero-point vibrational energies (ZPVEs) and enthalpic corrections were obtained from these calculations. The ZPVEs were scaled by 0.99 as recommended in refs. 85 and 86. All geometry optimization, frequency, computationally economical composite ab initio calculations were performed using the Gaussian 16 program suite.[87]

The above W1-F12 calculations are attainable for $(CH)_9$• radicals but are computationally too demanding for the larger $(CH)_{11}$• radicals. Thus, for the $(CH)_{11}$• radicals we use the computationally economical G4 thermochemical protocol.[88,89] The G4 method has been found to produce thermochemical properties of hydrocarbon cages,[59] barrier heights of pericyclic and cycloreversion reactions,[90,91] as well as other thermochemical and kinetic properties[58,61,88,89,92] with mean absolute deviations (MADs) from highly accurate experimental/theoretical data below the threshold of chemical accuracy (i.e., MADs below 1 kcal mol^{-1}).

Of particular relevance to the present work, G4 theory was found to give excellent performance for the reaction energies and barrier heights of Cope rearrangements in substituted bullvalenes.[21] Namely, relative to CCSD(T)/CBS values from W1-F12 theory, G4 attains an average root-mean-square deviation (RMSD) of 2.0 kJ mol^{-1} for a range of reaction energies and barrier heights. However, since this benchmark set considered closed-shell species, it is instructive to evaluate the performance of DFT and composite ab initio methods relative to the

W1-F12 reaction energy and barrier heights obtained for the $(CH)_9$• radicals in the present work. These results are summarized in Table 1. We consider here the DFT methods that were found to give good performance for the reaction energies and barrier heights in substituted bullvalenes,[21] namely PBE0,[93] B1B95,[94] BMK,[95] PW6B95,[96] and MN12-SX.[97] Table 1 shows that these DFT methods show deteriorated performance for the potential energy profile of the $(CH)_9$• rearrangement with RMSDs ranging between 14.5–16.5 kJ mol^{-1}. The composite ab initio procedures G4(MP2),[98] CBS-APNO,[99] and CBS-QB3[100] result in better performance, however, they still result in relatively large RMSDs ranging between 5.7–6.4 kJ mol^{-1}. Thus, these composite ab initio methods are not recommended for investigating the $(CH)_{11}$• rearrangements. However, consistent with the excellent performance of G4 theory for the closed-shell bullvalenes,[21] G4 theory results in good performance with an RMSD of 3.6 kJ mol^{-1} below the threshold of chemical accuracy. We therefore use G4 theory for investigating the reaction profiles involved in the $(CH)_{11}$• rearrangements.

Table 1. Statistical analysis for the performance of DFT and computationally economical composite ab initio procedures for the reaction energies and barrier heights involved in the $(CH)_9$• rearrangement relative to CCSD(T)/CBS reference values (in kJ mol^{-1}).[a]

	RMSD	MAD	MSD
BMK	16.5	16.1	–2.0
PBE0	15.5	15.2	–6.5
B1B95	15.2	15.2	–6.1
PW6B95	14.9	14.5	–1.4
MN12-SX	14.5	13.3	0.4
CBS-APNO	6.4	5.3	–4.0
G4(MP2)	6.0	5.7	–5.7
CBS-QB3	5.7	5.2	–4.0
G4	3.6	3.6	–3.6

[a]Root-mean-square deviation (RMSD), mean-absolute deviation (MAD), and mean-signed deviation (MSD) relative to CCSD(T)/CBS reference ΔH_{298} values from W1-F12 theory.

Results and Discussion

The unimolecular rearrangement of the barbaralyl radical $(CH)_9$• has been investigated via ^{1}H NMR and deuterium label experiments.[36,37,38] These experiments suggested that, in contrast to the closed-shell fluxional hydrocarbon cags (e.g., semibullvalene and bullvalene) which rearrange via a series of degenerate Cope rearrangements, the barbaralyl radical can undergo both Cope rearrangements and beta scission followed by cyclization steps to open and close the cyclopropyl ring. Deuterium label experiments conducted over 30 years ago suggest that the beta scissions are kinetically more favorable. Here, we use the high-level W1-F12 composite ab initio method to explore the potential energy surfaces of these competing reaction pathways. Figure 1 gives a schematic representation of the species located along the β-scission/cyclization and Cope rearrangement pathways. Both reaction pathways start from the barbaralyl radical in which the unpaired electron is located on the CH group connecting the bridgehead carbons (C_4 and C_8). As illustrated in Figure 1, the reaction pathway (β-scission/cyclization or Cope rearrangement) depends on which bond of the cyclopropane ring is being broken. β-Scission of either the C_1–C_8 or C_7–C_8 bond produces a stable bicyclo[3.2.2]nona-2,6,8-trienyl radical (hereinafter, trienyl radical), which has four possibilities for cyclization. Alternatively, breaking of the C_1–C_7 bond results in the Cope rearrangement (Figure 1).

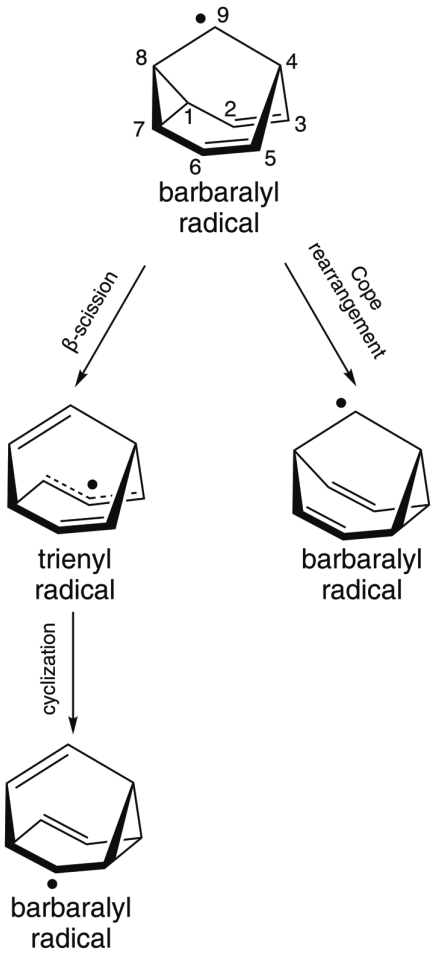

Figure 1. Schematic representation of possible species located along the $(CH)_9$• rearrangement channels via β-scission followed by cyclization or via Cope rearrangement.

Figure 2 gives the W1-F12 Gibbs free reaction profiles at 298 K (ΔG_{298}) for the two competing rearrangements of the $(CH)_9$• cages. The component breakdown of the W1-F12 reaction energies and barrier heights are given in Table S1 of the Supporting Information. Let us begin by examining the reaction profile for the rearrangement of the barbaralyl radical via β-scission and consecutive cyclization steps. β-Scission of either the C_1–C_8 or C_7–C_8 bonds of the cyclopropane ring produces a trienyl radical. Using electron spin resonance measurements, Walton[38] estimated that the activation barrier for this β-scission should be on the order of 5 kcal mol^{-1} (or about 21 kJ mol^{-1}). Our high-level W1-F12 results are consistent with this estimation,

namely we obtain a reaction barrier height of 25.3 kJ mol^{-1} relative to the barbaralyl radical on the ΔG_{298} potential energy surface. The formed trienyl radical lies 33.6 kJ mol^{-1} below the barbaralyl radical. Walton[38] also found that the barbaralyl and trienyl radicals are at equilibrium at ca. 100 °C with a dominant trienyl population. This experimental result is in qualitative agreement with the greater stability of the trienyl radical by 33.6 kJ mol^{-1} and with the reaction barrier heights for the interconversion between these two radicals, namely, $\Delta G_{298}^{\ddagger}$ = 25.3 and 58.9 kJ mol^{-1} in the forward and reverse directions (Figure 2). In the trienyl radical the unpaired electron is delocalized over the C_1–C_2–C_3 bridge as indicated from C_1–C_2 and C_2–C_3 bond distances of 1.386 Å (Figure 2). Thus, this radical is stabilized by allyl-type delocalization of the unpaired electron.

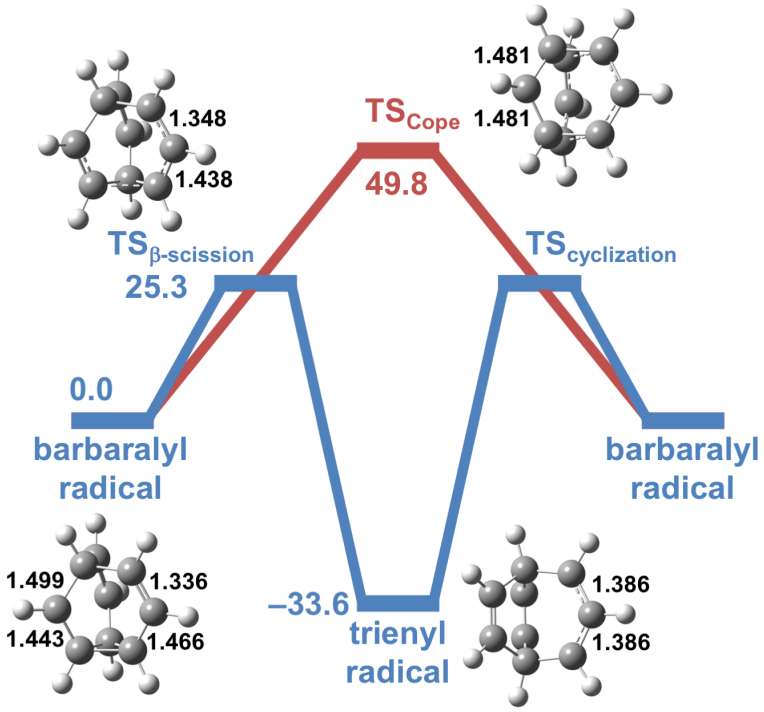

Figure 2. Gibbs free potential energy profiles for the rearrangement of $(CH)_9$• via β-scission and cyclization steps (blue curve, note that the β-scission and cyclization transition structures are energetically equivalent) and Cope rearrangement (red curve) (ΔG_{298}, W1-F12, kJ mol^{-1}). Selected bond distances are given in Å.

The W1-F12 Gibbs free reaction barrier height for the Cope rearrangement ($\Delta G_{298}^{\ddagger}$) is higher by 24.5 kJ mol^{-1} than the reaction barrier height for the β-scission (Figure 2). This energy difference between the two transition structures is partly attributed to the allyl-type delocalization of the unpaired electron present in the β-scission transition structure, but not the Cope rearrangement transition structure. Figure 3 gives natural population analysis (NPA) atomic spin densities on selected carbon atoms. In the transition structure for the Cope rearrangement the unpaired electron is localized on the methano bridge carbon (–HC•–) that connects the bridgehead carbons as evident from a spin density of 0.93 on this carbon. This transition structure has C_{2v} symmetry, and the symmetry equivalent C–C bonds around the radical center of 1.481 Å (Figure 2) also indicate that the unpaired electron is predominantly localized on the methano bridge carbon. For comparison, in the barbaralyl reactant the spin density on this carbon is 0.86 and the lengths of the corresponding C–C bonds are 1.443 and 1.499 Å (Figure 2). In the transition structure for the β-scission, on the other hand, the unpaired electron is delocalized over two of the three hydrocarbon bridges connecting the bridgehead carbons. In particular, we obtain spin densities of 0.59 on the two-carbon bridge, and a spin density of 0.58 delocalized between the two carbons on the three-carbon bridge which benefits from allyl-type delocalization (Figure 3). The allyl-type delocalization of the unpaired electron over the three-carbon bridge is also evident from C–C bond distances of 1.438 and 1.348 Å (see Figure 2). Thus, the relative stability of the transition structure for the β-scission is partly attributed to the larger degree of delocalization of the unpaired electron.

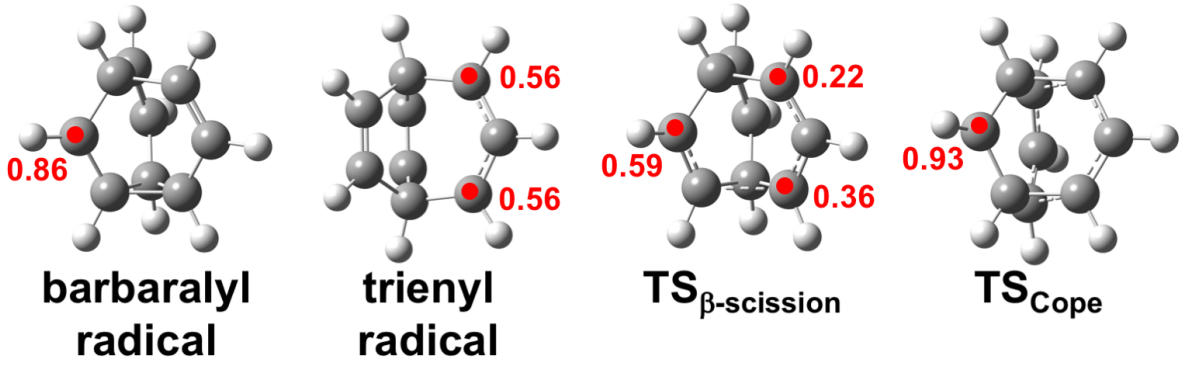

Figure 3. Natural population analysis (NPA) spin densities on selected carbon atoms calculated at the B3LYP-D3/Def2-TZVPP level of theory.

The above results show that there is a kinetic preference for the β-scission/cyclization pathway over the Cope rearrangement pathway in the $(CH)_9$• radical. We proceed to examine these competing reaction pathways in the larger $(CH)_{11}$• radical cage. We note that ref. 38 suggested that this rearrangement would be slower than in the $(CH)_9$• radical, however, to the best of our knowledge, to date this system has not been synthesized or studied computationally. In contrast to the reaction profiles in the $(CH)_9$• radical which involve only two kinetically accessible local minima, for the $(CH)_{11}$• radical we located five local minima that are kinetically accessible. Figure 4 shows a schematic representation of the local minima that were located along the β-scission/cyclization and Cope rearrangement pathways.

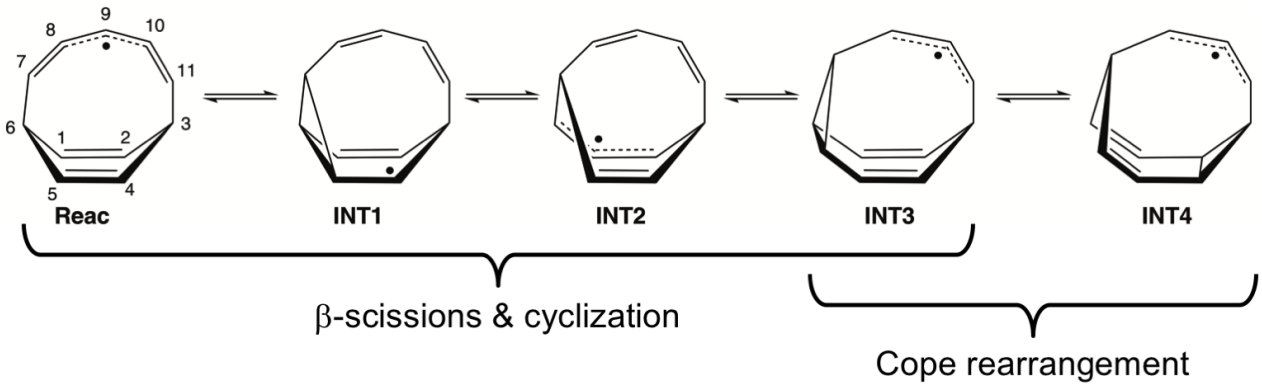

Figure 4. Schematic representation of the local minima located along the $(CH)_{11}$• rearrangement channels via β-scission/cyclization steps and Cope rearrangement.

Figure 5 gives the G4 Gibbs free reaction profiles at 298 K for the β-scission/cyclization and Cope rearrangement pathways in the $(CH)_{11}$• cage. Let us begin by examining the reaction profile for the rearrangement via β-scission and consecutive cyclization steps. This reaction profile involves four hydrocarbon cages – two minima without a cyclopropane ring (**Reac** and **INT2**) and two minima with a strained cyclopropane ring (**INT1** and **INT3**). The reactant (**Reac**, Figures 4 and 5) involves a 5-carbon bridge connecting the two sp^3 bridgehead carbons, whilst **INT2** involves a 4-carbon bridge connecting the two sp^3 bridgehead carbons. The energetic stability of the reactant relative to **INT2** by 18.4 kJ mol^{-1} may be partly explained by the smaller strain energy associated with the longer hydrocarbon bridge. Figure 6 gives NPA atomic spin densities on selected carbon atoms. In the reactant (**Reac**) the free radical is delocalized over the entire 5-carbon bridge, whereas in **INT2** it is mainly localized on two non-conjugated carbons of the 7-membered ring. Thus, the delocalization of the free radical in the reactant may contribute to its relative stability. The two intermediates which involve a strained cyclopropane ring lie 63.3 (**INT1**) and 27.3 (**INT3**) kJ mol^{-1} above the reactant. The relatively high energy of **INT1** may be attributed to the cyclopropane ring being a fused bicyclic (3:6) ring system compared to the less strained (3:7) ring system in **INT3**. In addition, the free radical in **INT3** is cantered mainly on a

single sp^3 carbon, whereas in **INT3** the unpaired electron is delocalized over the 3-carbon allylic bridge (Figure 6).

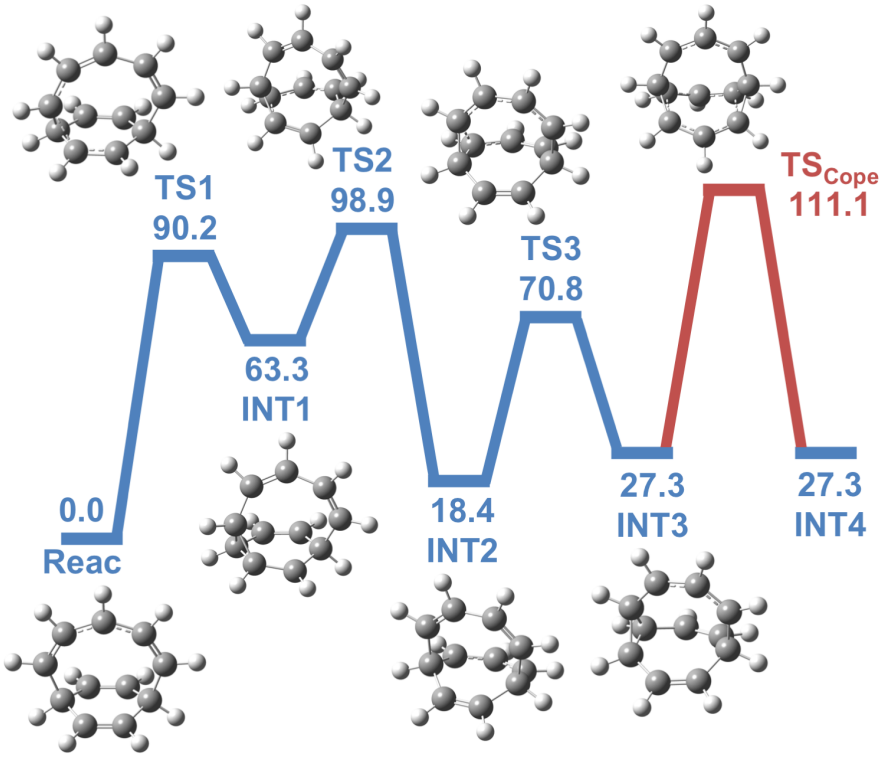

Figure 5. Gibbs free potential energy profiles for the $(CH)_{11}$• rearrangement via β-scission and cyclization steps (blue curve) and Cope rearrangement (red curve) (ΔG_{298}, G4, kJ mol^{-1}).

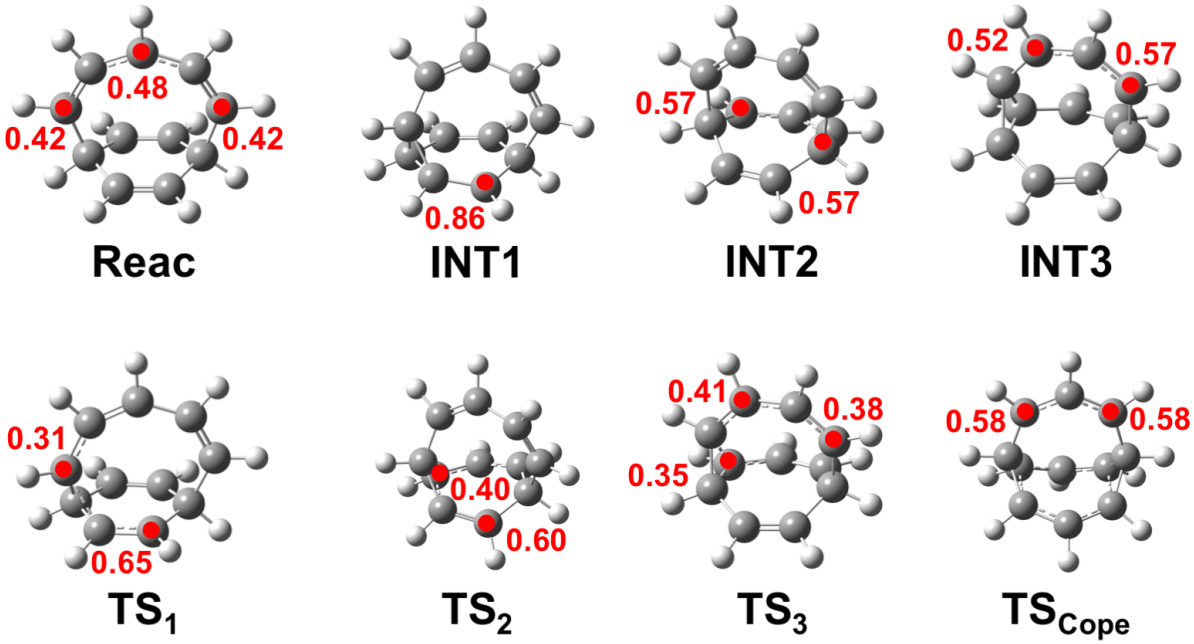

Figure 6. Natural population analysis (NPA) spin densities on selected carbon atoms calculated at the B3LYP-D3/Def2-TZVPP level of theory.

The transition structures involved in the β-scission/cyclization pathway (**TS1**, **TS2**, and **TS3**) lie 90.2, 98.9, and 70.8 kJ mol^{-1} above the reactant. All three transition structures involve opening or closing of the stained cyclopropyl ring. However, whilst in **TS1** and **TS2** the partially formed cyclopropyl ring is fused to a six-membered ring, in **TS3** it is fused to a seven-membered ring. Thus, the latter transition structure is expected to involve less strain. In addition, in **TS3** the unpaired electron is delocalized over three carbon atoms, which may further contribute to its relative stability compared to **TS1** and **TS2** where the unpaired electron is delocalized over two carbon atoms. Overall, the β-scission/cyclization and Cope rearrangement pathways involve similar rate determining steps with Gibbs free activation barriers of 98.9 and 111.1 kJ mol^{-1}, respectively (Figure 5). Thus, the kinetic preference for β-scission/cyclization over Cope rearrangement is diminished in the $(CH)_{11}$• cages relative to that in the $(CH)_{9}$• cages. In addition, the barriers for the β-scission/cyclization and Cope rearrangements in $(CH)_{11}$• are higher by 30–

40 kJ mol^{-1} than the corresponding barriers in $(CH)_9$• indicating that the former cage would require a higher temperature to achieve full fluxionality.

Conclusions

Using the high-level W1-F12 composite ab initio method, we brush the dust off the intriguing rearrangement of the shapeshifting barbaralyl radical $(CH)_9$•. We find that consistent with the experimental results, the barbaralyl radical rearranges through a series of β-scission and cyclization steps rather than degenerate Cope rearrangements. In particular, we calculate Gibbs free activation energies ($\Delta G_{298}^{\ddagger}$) of 25.3 and 49.8 kJ mol^{-1} for the cyclopropyl ring-opening step and Cope rearrangement, respectively relative to the barbaralyl radical. We proceed to examine these chemical processes in a the larger $(CH)_{11}$• shapeshifting radical cage, which has not been experimentally synthesized. This shapeshifting radical involves a more complex set of rearrangements through β-scissions and cyclizations and is predicted to be less fluxional than the barbaralyl radical.

Supplementary data

Component breakdown of the W1-F12 reaction energies and barrier heights for the $(CH)_9$• rearrangements (Table S1); Optimized geometries for the species considered in this work (Table S2); and full references for Molpro 2016 and Gaussian 16.

Acknowledgments

This work is dedicated to Prof. Leo Radom and his lifelong work on free radicals. This research was undertaken with the assistance of resources from the National Computational Infrastructure

(NCI), which is supported by the Australian Government. We also acknowledge the system administration support provided by the Faculty of Science at the University of Western Australia to the Linux cluster of the Karton group.

Funding Information

Australian Research Council (ARC) Future Fellowship (Project No. FT170100373).

References

[1] W. v. E. Doering, W. R. Roth, Tetrahedron, 19 (1963) 715.

[2] G. Schröder, Angew. Chem. Int. Ed. Eng. 2 (1963) 481.

[3] A. N. Bismillah, B. M. Chapin, B. A. Hussein, P. R. McGonigal, Chem. Sci. 11 (2020) 324.

[4] A. G. Császár, C. Fábri1, J. Sarka, WIREs Comput Mol Sci.10 (2020) e1432.

[5] N. Graulich, WIREs Comput. Mol. Sci. 1 (2011) 172.

[6] M. L. McKee, WIREs Comput. Mol. Sci. 1 (2011) 943.

[7] A. Adult, J. Chem. Educ. 78 (2001) 924.

[8] M. Khojandi, A. Seif, E. Zahedi, L. R. Domingo, M. Karimkhani. New J. Chem. 44 (2020) 6543.

[9] H. D. Patel, T.-H. Tran, C. J. Sumby, L. F. Pašteka, T. Fallon, J. Am. Chem. Soc. 142 (2020) 3680.

[10] O. Yahiaoui, L. F. Pasteka, C. J. Blake, C. G. Newton, T. Fallon, Org. Lett. 21 (2019) 9574.

[11] S. Ferrer, A. M. Echavarren, Synthesis 51 (2019) 1037.

[12] O. Yahiaoui, L. F. Pasteka, B. Judeel, T. Fallon, Angew. Chem. Int. Ed. 57 (2018) 2570.

[13] A. N. Bismillah, J. Sturala, B. M. Chapin, D. S. Yufit, P. Hodgkinson, P. R. McGonigal, Chem. Sci. 9 (2018) 8631.

[14] M. He, J. W. Bode, Proc. Natl. Acad. Sci. U.S.A. 108 (2011) 14752.

[15] J. F. Teichert, D. Mazunin, J. W. Bode, J. Am. Chem. Soc. 135 (2013) 11314.

[16] A. R. Lippert, V. L. Keleshian, J. W. Bode, Org. Biomol. Chem. 7 (2009) 1529.

[17] A. R. Lippert, J. Kaeobamrung, J. W. Bode, J. Am. Chem. Soc. 128 (2006) 14738.

[18] R. Poupko, H. Zimmermann, K. Müller, Z. Luz, J. Am. Chem. Soc. 118 (1996) 7995.

[19] S. Kozuch, T. Schleif, A. Karton. Phys. Chem. Chem. Phys. 23 (2021) 10888.

[20] Z. Shadfar, O. Yahiaoui, T. A. Collier, T. Fallon, J. R. Allison, J. Chem. Phys. 154 (2021) 154105.

[21] A. Karton, Chem. Phys. 540 (2021) 111013.

[22] A. Karton, Chem. Phys. Lett. 759 (2020) 138018.

[23] Y. J. Okamoto, Chem. Phys. 150 (2019) 134103.

[24] Y.-Y. Ma, M. Yan, H.-R. Li, Y.-B. Wu , X.-X. Tian, H.-G. Lu, S.-D. Li, Sci. Rep. 9 (2019) 17074.

[25] D. Sharma, M. Ojha, P. Maheshwari, A. Gurjar, R. K. Bansal, Phosphorus Sulfur. 190 (2015) 1.

[26] T. Bredtmann, B. Paulus, J. Chem. Theory Comput. 9 (2013) 3026.

[27] M. He, J. W. Bode, Org. Biomol. Chem. 11 (2013) 1306.

[28] P. R. Griffiths, D. E. Pivonka, R. V. Williams, Chem. Eur. J. 17 (2011) 9193.

[29] X. Zhang, D. A. Hrovat, W. T. Borden, Org. Lett. 12 (2010) 2798.

[30] T. Rozgonyi, A. Bartok-Partay, A. Stirling, J. Phys. Chem. A 114 (2010) 1207.

[31] E. C. Brown, R. F. W. Bader, N. H. Werstiuk, J. Phys. Chem. A 113 (2009) 3254.

[32] S. C. Wang, D. J. Tantillo, J. Phys. Chem. A, 111 (2007) 7149.

[33] D. A. Hrovat, E. C. Brown, R. V. Williams, H. Quast, W. T. Borden, J. Org. Chem. 70 (2005) 2627.

[34] H.-S. Wu, H. Jiao, Z.-X. Wang, P. v. R. Schleyer, J. Am. Chem. Soc. 125 (2003) 10524.

[35] E. C. Brown, D. K. Henze, W. T. Borden, J. Am. Chem. Soc. 124 (2002) 14977.

[36] W. N. Washburn, J. Am. Chem. Soc. 100 (1978) 6235.

[37] J. C. Walton, J. Chem. Soc., Chem. Commun. (1989) 468.

[38] J. C. Walton, J. Chem. Soc., Perkin Trans. 2 (1989) 2169.

[39] S. Grimme, P. R. Schreiner, Angew. Chem. Int. Ed. 56 (2017) 2.

[40] A. Jain, Y. Shin, K. A. Persson, Nat. Rev. Mater. 1 (2016) 15004.

[41] Q. Tang, Z. Zhou, Z. Chen, WIREs Comput. Mol. Sci. 5 (2015) 360.

[42] D. J. Tantillo, Nat. Prod. Rep. 30 (2013) 1079.

[43] P. Pyykkö, Phys. Chem. Chem. Phys. 14 (2012) 14734.

[44] N. Radić, Z. B. Maksić, J. Org. Chem. 84 (2019) 2425.

[45] C. Elgindy, J. S. Ward, M. S. Sherburn, Angew. Chem. Int. Ed. 58 (2019) 14573.

[46] W. D. Allen, H. Quanz, P. R. Schreiner, J. Chem. Theory Comput. 12 (2016) 4707.

[47] D. Sundholm, Phys. Chem. Chem. Phys. 15 (2013) 9025.

[48] D. Sundholm, L. N. Wirz, P. Schwerdtfeger, Nanoscale 7 (2015) 15886.

[49] S. Grimme, Chem. Eur. J. 10 (2004) 3423.

[50] H. Wolf, D. Leusser, M. R. V. Jørgensen, R. Herbst-Irmer, Y.-S. Chen, E.-W. Scheidt, W. Scherer, B. B. Iversen, D. Stalke, Chem. Eur. J. 20 (2014) 7048.

[51] V. Parasuk, J. Almlof, M. W. Feyereisen, J. Am. Chem. Soc. 113 (1991) 1049.

[52] K. Kaiser, L. M. Scriven, F. Schulz, P. Gawel, L. Gross, H. L. Anderson, Science 365 (2019) 1299.

[53] A. Karton, J. M. L. Martin, J. Chem. Phys. 136 (2012) 124114.

[54] S. C. Wang, D. J. Tantillo, J. Phys. Chem. A 111 (2007) 7149.

[55] C. Hättig, W. Klopper, A. Köhn, D. P. Tew, Chem. Rev. 112 (2012) 4.

[56] A. Karton, WIREs Comput. Mol. Sci. 6 (2016) 292.

[57] A. Karton, S. Daon, J. M. L. Martin, Chem. Phys. Lett. 510 (2011) 165.

[58] A. Karton, N. Sylvetsky, J. M. L. Martin, J. Comput. Chem. 38 (2017) 2063.

[59] A. Karton, P. R. Schreiner, J. M. L. Martin, J. Comput. Chem. 37 (2016) 49.

[60] A. Karton, J. Phys. Chem. A 123 (2019) 6720.

[61] C. D. Smith, A. Karton, J. Comput. Chem. 41 (2020) 328.

[62] K. A. Peterson, T. B. Adler, H.-J. Werner, J. Chem. Phys. 128 (2008) 084102.

[63] J. Noga, S. Kedžuch, J. Šimunek, J. Chem. Phys. 127 (2007) 034106.

[64] G. Knizia, H.-J. Werner, J. Chem. Phys. 128 (2008) 154103.

[65] T. B. Adler, G. Knizia, H.-J. Werner, J. Chem. Phys. 127 (2007) 221106.

[66] J. M. L. Martin, G. Oliveira, J. Chem. Phys. 111 (1999) 1843.

[67] T. H. Dunning, J. Chem. Phys. 90 (1989) 1007.

[68] R. A. Kendall, T. H. Dunning, R. J. Harrison, J. Chem. Phys. 96 (1992) 6796.

[69] E. Papajak, D. G. Truhlar, J. Chem. Theory Comput. 7 (2011) 10.

[70] K. A. Peterson, T. H. Dunning, J. Chem. Phys. 117 (2002) 10548.

[71] M. Douglas, N. M. Kroll, Ann. Phys. 82 (1974) 89.

[72] B. A. Hess, Phys. Rev. A 33 (1986) 3742.

[73] W. A. de Jong, R. J. Harrison, D. A. Dixon, J. Chem. Phys. 114 (2001) 48.

[74] MOLPRO is a package of ab initio programs written by H.-J. Werner, P. J. Knowles, G. Knizia, F. R. Manby, M. Schütz, P. Celani, T. Korona, R. Lindh, A. Mitrushenkov, G. Rauhut, et al. See: http:www.molpro.net.

[75] C. Lee, W. Yang, R. G. Parr, Phys. Rev. B 37 (1988) 785.

[76] A. D. Becke, J. Chem. Phys. 98 (1993) 5648.

[77] P. J. Stephens, F. J. Devlin, C. F. Chabalowski, M. J. Frisch, J. Phys. Chem. 98 (1994) 11623.

[78] S. Grimme, S. Ehrlich, L. Goerigk, J. Comput. Chem. 32 (2011) 1456.

[79] F. Weigend, R. Ahlrichs, Phys. Chem. Chem. Phys. 7 (2005) 3297.

[80] S. Grimme, J. Antony, S. Ehrlich, H. Krieg, J. Chem. Phys. 132 (2010) 154104.

[81] S. Grimme, WIREs Comput. Mol. Sci. 1 (2011) 211.

[82] E. R. Johnson, A. D. Becke, J. Chem. Phys. 124 (2006) 174104.

[83] C. Gonzalez, H. B. Schlegel, J. Chem. Phys. 90 (1989) 2154.

[84] C. Gonzalez, H. B. Schlegel, J. Chem. Phys. 94 (1990) 5523.

[85] A. Karton, L.-J. Yu, M. K. Kesharwani, J. M. L. Martin, Theor. Chem. Acc. 133 (2014) 1483.

[86] M. K. Kesharwani, B. Brauer, J. M. L. Martin. J. Phys. Chem. A 119 (2015) 1701.

[87] M. J. Frisch, G. W. Trucks, H. B. Schlegel, G. E. Scuseria, M. A. Robb, J. R. Cheeseman, G. Scalmani, V. Barone, B. Mennucci, G. A. Petersson, et al. Gaussian 16, Revision A.03; Gaussian, Inc.: Wallingford CT, 2016.

[88] L. A. Curtiss, P. C. Redfern, K. Raghavachari, J. Chem. Phys. 126 (2007) 084108.

[89] L. A. Curtiss, P. C. Redfern, K. Raghavachari, WIREs Comput. Mol. Sci. 1 (2011) 810.

[90] L.-J. Yu, F. Sarrami, R. J. O'Reilly, A. Karton, Chem. Phys. 458 (2015) 1.

[91] A. Karton, L. Goerigk, J. Comput. Chem. 36 (2015) 622.

[92] L. A. Curtiss, P. C. Redfern, K. Raghavachari, Chem. Phys. Lett. 499 (2010) 168.

[93] C. Adamo, V. Barone, J. Chem. Phys. 110 (1999) 6158.

[94] A. D. Becke, J. Chem. Phys. 104 (1996) 1040.

[95] A. D. Boese, J. M. L. Martin, J. Chem. Phys. 121 (2004) 3405.

[96] Y. Zhao, D. G. Truhlar, J. Phys. Chem. A 109 (2005) 5656.

[97] R. Peverati, D. G. Truhlar, Phys. Chem. Chem. Phys. 14 (2012) 16187.

[98] L. A. Curtiss, P. C. Redfern, K. Raghavachari, J. Chem. Phys. 127 (2007) 124105.

[99] J. W. Ochterski, G. A. Petersson, J. A. Montgomery Jr., J. Chem. Phys. 104 (1996) 2598.

[100] J. A. Montgomery Jr, M. J. Frisch, J. W. Ochterski, G. A. Petersson, J. Chem. Phys. 110 (1999) 2822.

Graphical TOC